

Visible-light responsive TiO₂ for the complete photocatalytic decomposition of volatile organic compounds (VOCs) and its efficient acceleration by thermal energy

Kosuke Imai ^a, Takashi Fukushima ^a, Hisayoshi Kobayashi ^b, Shinya Higashimoto ^{a,*}

^a Department of Applied Chemistry, Faculty of Engineering, Osaka Institute of Technology, 5-16-1 Omiya, Asahi-ku, Osaka 535-8585, Japan

^b Emeritus professor of Kyoto Institute of Technology, Matsugasaki, Sakyo-ku, Kyoto 606-8585, Japan

ARTICLE INFO

Keywords:

Visible-light responsive TiO₂
Decomposition of VOCs
Interfacial surface complex (ISC)
Photothermal catalysis
TiO₂ {001} facet

ABSTRACT

Titanium dioxide (TiO₂) semiconductors are known to exhibit photocatalysis by bandgap excitation upon UV-light ($h\nu > 3.2$ eV) irradiation. TiO₂ has been extensively investigated in the challenge to address the urgent need for environmental remediation such as the degradation of volatile organic compounds (VOCs). In this study, it was striking that the TiO₂ exhibited effective reactivity for the complete degradation of various VOCs such as benzene, toluene and m-xylene (BTX) into CO₂ under visible-light irradiation (2.3 eV $< h\nu$). This is because the adsorption of various VOCs on TiO₂ results in the formation of an interfacial surface complex (ISC) that provides weak light absorption in the visible light region. In particular, the correlation between the apparent quantum yields in the photocatalytic decomposition of toluene and the light absorption wavelengths of the ISC was clearly demonstrated. By density functional theory (DFT) simulations, the mechanism for origin of the visible-light responsive TiO₂ was clarified. Furthermore, thermal effects on the visible-light responsive TiO₂ photocatalysis were investigated. It was found that the combination of visible light-energy and its excess thermal energy significantly enhanced activity for the degradation of toluene.

1. Introduction

Titanium dioxide (TiO₂) is one of the most practical photo-functional materials since it is chemically stable, abundant (Ti: 10th highest Clark number), non-toxic, and cost efficient. In recent years, much attention has been focused on the use of TiO₂ semiconductive photocatalysts for the mineralization of toxic substances in polluted air and water, organic synthesis, and artificial photosynthesis to produce fuels [1–6]. The valence band (VB) and conduction band (CB) of TiO₂ mainly consist of O 2p and Ti 3d orbitals, respectively. TiO₂ exhibits bandgaps at 3.2 eV for the anatase and 3.0 eV for the rutile structures. UV-light irradiation of the TiO₂ photocatalyst induced electrons on the CB and holes on the VB, enabling the reduction and oxidation of the reactants, respectively. Photocatalytic decomposition of VOCs such as toluene into CO₂ was extensively investigated on TiO₂ photocatalyst in air under UV-light irradiation [7–11]. The photocatalytic activities of TiO₂ strongly depend on intrinsic physicochemical properties such as their crystal structures [12–14], crystallinity [15,16], crystalline facets [17–19], particle sizes [20–22] and defective sites [23–27]. It was previously

reported that the exposed {101} and {001} facets on anatase TiO₂ affect the photocatalytic activity [28]. In particular, the {001} facet was considered to show higher photocatalytic activity than the {101} facet due to having more undercoordinated Ti_{5c} centers and higher surface energy [29–34].

It is known that TiO₂ operates under UV-light irradiation of a small fraction (4%) of the solar energy reaching the earth's surface. Therefore, the design and development of visible light-driven photocatalysts that can utilize as much solar energy as possible, including 50% visible light, is an urgent and important goal [2,6,35,36]. To improve the reaction activity of TiO₂ photocatalysts, the light absorption wavelength needs to be extended. The following strategies are shown for fabrication of visible-light responsive TiO₂. The introduction of heteroatoms such as nitrogen (N) into the bulk TiO₂ [35,36], or surface modification with Fe³⁺ ions [37,38] and organic compounds such as catechol [39] exhibit visible light absorption, resulting in the photocatalytic reactions such as decomposition of volatile organic compounds (VOCs) into CO₂, and water splitting to form H₂. Another concept is the formation of interfacial surface complexes (ISC) through the interaction of reactant

* Corresponding author.

E-mail address: shinya.higashimoto@oit.ac.jp (S. Higashimoto).

molecules with TiO_2 surfaces, which are converted into products liberated from the TiO_2 surface under visible light irradiation. It was previously reported that the interaction of reactant molecules such as benzyl alcohol with TiO_2 formed the alcoholate species as the ISC, in which excitation with visible-light in the presence of O_2 was found to selectively convert into benzaldehyde [40–42]. For the complete decomposition of formic acid, Ariga et al. have reported that the rutile TiO_2 single crystal with (001) facet interacting with formic acid made the bandgap significantly smaller than 3.0 eV, resulting in the surface-mediated visible light-induced photo-oxidation of formic acid into CO_2 [43]. Interestingly, Ren et al. have reported that the TiO_2 (001) facet on home-made nanosheets exhibited the photocatalytic decomposition of benzene or acetone into CO_2 under visible light irradiation [44]. However, as far as we know, the photocatalytic decomposition of various aromatic and aliphatic compounds have been few investigated under visible light irradiation on commercially available TiO_2 photocatalysts by itself without bulk/or surface modification. The complete photodegradation of VOCs into CO_2 , in particular, persistent benzene, toluene and xylene (BTX) has attracted much attention in recent years.

In this study, the complete decomposition of VOCs such as BTX into CO_2 under visible-light irradiation using a TiO_2 photocatalyst was undertaken. In particular, the origin of the visible light response of TiO_2 for the decomposition of toluene was investigated by UV-Vis spectroscopy, apparent quantum yields, FT-IR spectroscopy and computational simulations by density functional theory (DFT). Furthermore, the thermal effect on the photocatalytic activity of TiO_2 under visible-light irradiation was studied to clarify the factors that lead to the effective use of the heat generated by the light source.

2. Experimental section

2.1. Photocatalytic reactions

In these experiments, TiO_2 (ST-01) from Ishihara Sangyo Kaisha, Ltd. was used as the photocatalyst unless otherwise noted. Prior to photocatalytic reactions and spectroscopic measurements, the photocatalysts were calcined at 300 °C for 1 h in air. The photocatalyst (20 mg) was spread on the flat bed of a pyrex cell (area photo-irradiated: 3.46 cm², volume: 10 cm³) in a reactor and the gas phase was purged by O_2 capped with a precision seal septa. The undiluted solutions of VOCs (0.1 or 1.0 μL) were subsequently introduced into the cell by a syringe and vaporized. Light was irradiated from the bottom of the pyrex cell. Visible light was irradiated with LED lamps (blue: 420 < λ < 520 nm, green: 450 < λ < 600 nm; and red: 620 < λ < 720 nm, OptiLED, 2.5 W, IMPACT EYE Co., Ltd). Profiles for the photo-energy emitted from the LED lamps are shown in Fig. SI 1. The photo-intensity of the LED lamps was measured by an illumination meter (DT-1309, CEM Co., Ltd.), and the photo-intensities of the blue, green and red lights were adjusted to 1.1×10^5 lx unless otherwise noted, and the reaction temperature was fixed at 40°C. The amounts of CO_2 evolved in the reactions were measured using a gas chromatograph (GC-8A, Shimadzu, Japan, column: porapak Q). After the reaction, the intermediate species adsorbed on the photocatalyst were extracted by acetonitrile. The solution was, then, analyzed by HPLC (Shimadzu LC10ATVP, UV-Vis detector, column: Chemcopak, mobile phase: a mixture of acetonitrile and 1.0% formic acid aqueous solution in the ratio of 3: 7 in volume), and benzaldehyde was identified.

For the estimation of the apparent quantum yields, the photocatalyst (50 mg) was spread on the flat bed of a pyrex cell in a reactor and the gas phase was purged by O_2 capped with a precision seal septa. The liquid toluene (1.0 μL) was subsequently introduced into the cell by a syringe and vaporized. The photocatalyst was irradiated with various monochromatic light through a xenon lamp (LAX-C100, Asahi spectra) equipped with various bandpass filters (Asahi spectra). The full width at half maximum (FWHM) of each photo-irradiated wavelength was ca. 13.6 nm and the photo-energy was measured by a power-meter (ORION/PD, Ophir). Assuming a 36-electron reaction over the ionic

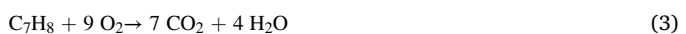
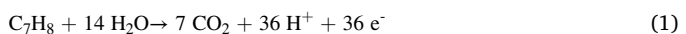
Table 1

CO_2 evolution for the decomposition of various VOCs on TiO_2 under visible light irradiation emitted from the blue lamp.

| VOC | $\text{CO}_2/\mu\text{mol}$ | Decomposition ratio / % |
|-------------------|-----------------------------|-------------------------|
| benzene | 6.1 | 14.7 |
| toluene | 7.1 | 10.7 |
| m-xylene | 8.3 | 12.7 |
| benzyl alcohol | 26.1 | 38.6 |
| ethanol | 3.8 | 11.1 |
| formaldehyde | 5.8 | 42.4 |
| benzaldehyde | 26.3 | 38.1 |
| acetaldehyde | 5.7 | 17.6 |
| acetic acid | 6.0 | 17.2 |
| methylcyclohexane | 3.4 | 6.2 |

Amounts of VOC (1.0 μL) added; Reaction time (20 h).

reaction formula (1) and (2) for the complete decomposition of toluene to CO_2 (3), the apparent quantum yield (Φ) was calculated in the following Eq. (4):



$$\Phi (\%) = \frac{(\text{amount of product formed}/\mu\text{mol}) \times 36}{(\text{amount of photons induced}/\mu\text{mol})} \times 100 \quad (4)$$

2.2. Characterizations

The X-ray diffraction (XRD) patterns were obtained with a RIGAKU RINT2000 using $\text{Cu K}\alpha$ radiation ($\lambda = 1.5417 \text{ \AA}$) at a voltage of 20 kV and a current of 2 mA. UV-Vis spectroscopic measurements were carried out by diffuse reflectance with a UV-Vis scanning spectrophotometer (UV-3600, Shimadzu). The absorbance of the samples was recorded using barium sulfate (BaSO_4) as the reference. The IR spectra of the solids were measured by FT-IR spectroscopy (IRAffinity-1S, Shimadzu) in the reflection mode with MIRacleA (ZnSe) and recorded with 100 scans at 4 cm⁻¹ resolution. Analyses of the chemical composition and binding energy were carried out by an X-ray photoelectron spectroscope (XPS, JPS-9030, JEOL Ltd.) attached with a Mg K α X-ray (1253.6 eV) operating at an energy of 100 W (10 mA × 10 kV). The binding energies were corrected against C 1 s (285 eV).

2.3. Computational calculation by density functional theory (DFT)

The electronic structure of each slab model was calculated by the plane-wave based DFT program Castep [45]. The Perdew, Burke and Ernzerhof (PBE) functional [46] was used together with the ultra-soft core potentials for optimization [47] and the norm conserving core potentials for post-energy refinement [48]. Semi-empirical dispersion interaction correction was also employed [49]. The basis set cut-off energy was adjusted to 300 and 750 eV for optimization and post-energy calculations, respectively. The electron configurations of the atoms were Ti: 3 s²3p⁶4 s²3d², H: 1 s¹, C: 2 s²2p² and O: 2 s²p⁴. All the atomic coordinates were optimized, and the lattice constants were fixed to the one derived from the crystalline structure of anatase. The anatase {101} and {001} crystal facets were modeled by the $(\text{TiO}_2)_6$ and $(\text{TiO}_2)_3$ slab unit cells, respectively, which were used for calculation of the projected density of states (PDOS) of TiO_2 . The $(\text{TiO}_2)_{36}$ and $(\text{TiO}_2)_{27}$ super cells which were extended by (2 × 3) times of $(\text{TiO}_2)_6$ and (3 × 3) times of $(\text{TiO}_2)_3$, respectively, were employed to avoid the overlapping between toluene molecules.

The additional experimental sections for the “Materials” and “Sample preparation” are described in the Supporting Information.

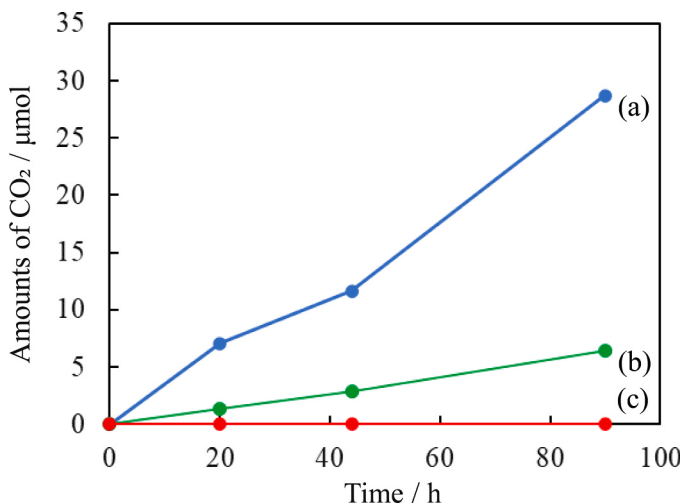


Fig. 1. Time profiles for the photocatalytic decomposition of toluene (1.0 μL) under illumination from (a) blue, (b) green, and (c) red LED lamps.

3. Results and discussion

3.1. Photocatalytic decomposition of various VOCs on TiO₂

The photocatalytic decomposition of various kinds of VOCs into CO₂ in the presence of O₂ on the TiO₂ photocatalyst was investigated under visible light irradiation emitted from the blue LED lamp and the results are shown in Table 1. It was confirmed that decomposition does not take place under photo-irradiation without a photocatalyst nor with a photocatalyst without irradiation, i.e., both photocatalyst and irradiation are required in combination for the reaction to occur. Photodegradation of VOCs (aromatic and aliphatic hydrocarbons, alcohols, aldehydes and carboxylic acids) shown in Table 1 was carried out on TiO₂ photocatalysts under visible light irradiation, leading to CO₂ generation in all systems. It was striking that the TiO₂ exhibited effective reactivity for the complete degradation of various VOCs into CO₂ under visible-light irradiation.

In this study, the photocatalytic performance of visible-light responsive TiO₂ for the decomposition of aromatic hydrocarbons, in particular BTX, was examined. As shown in Fig. 1, when the decomposition of toluene on TiO₂ was performed under visible-light irradiation emitted from the blue LED lamp, the amount of CO₂ increased with an

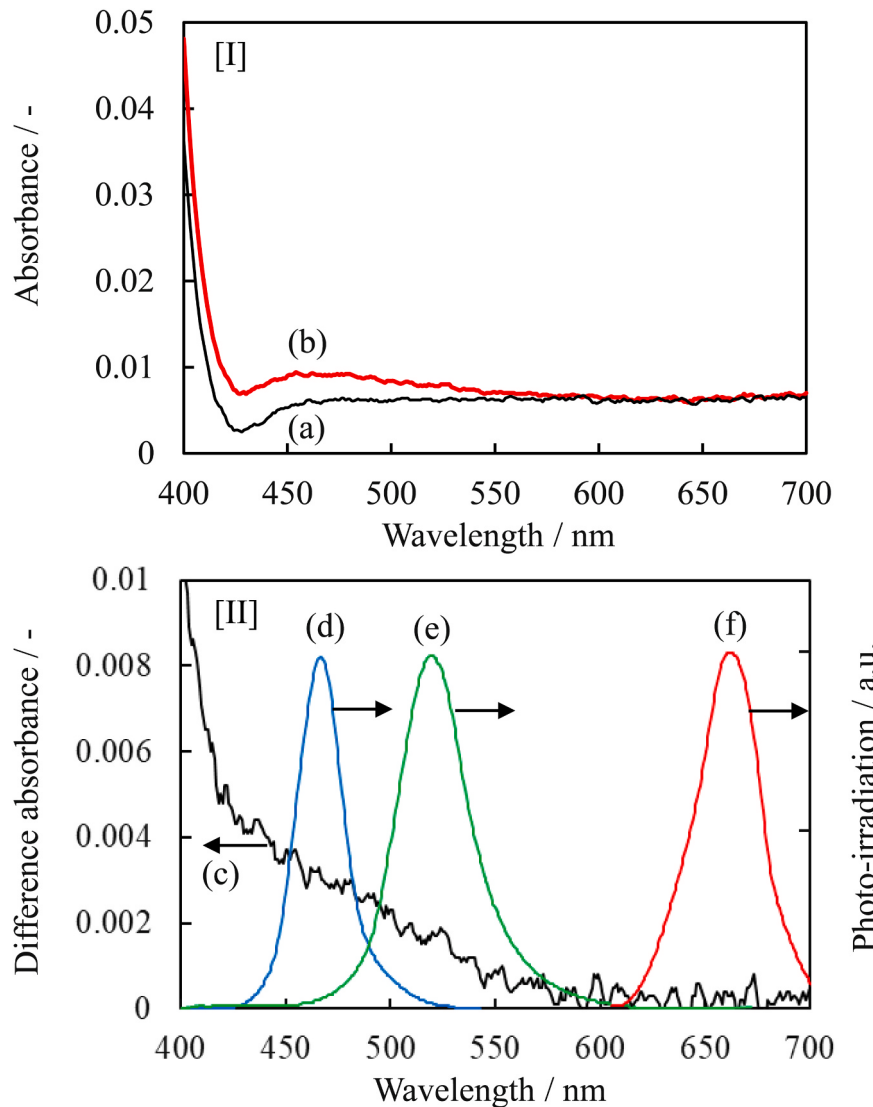


Fig. 2. UV-Vis spectra [I] of (a) TiO₂ and (b) TiO₂ adsorbed toluene, and [II] (c) their difference spectrum, and the light-energy distribution from (d) blue, (e) green and (f) red LED lamps.

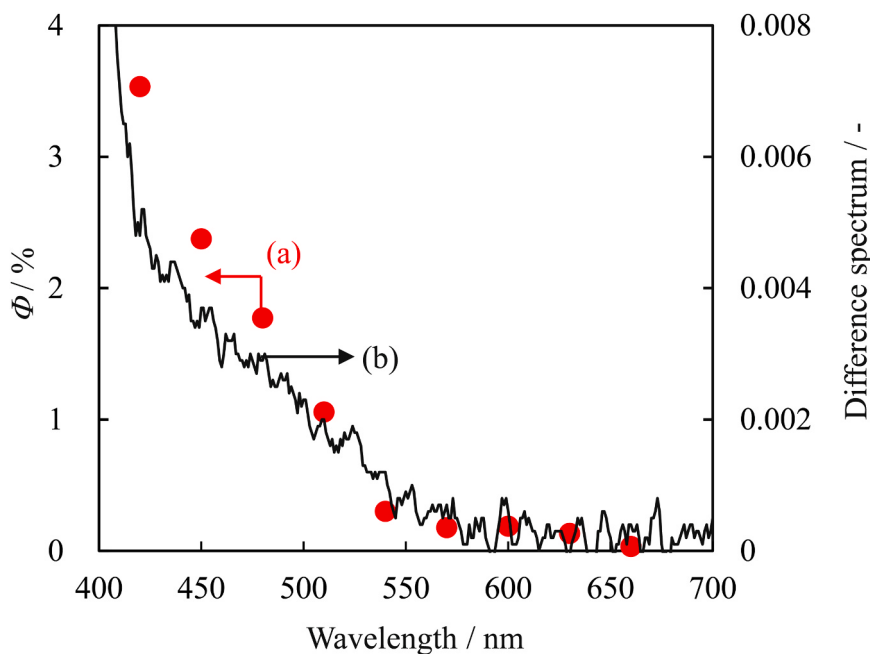


Fig. 3. Relationship between apparent quantum yields (a) for the photocatalytic decomposition of toluene and (b) difference spectrum subtracting TiO_2 from toluene-adsorbed TiO_2 .

increase in the irradiation time, while irradiation from the green lamp produced small amounts of CO_2 . When irradiated from a red lamp, CO_2 could hardly be formed on the TiO_2 . It was noted that a small amount of CO_2 was evolved when TiO_2 itself was exposed to light in the absence of the reactant molecules due to the decomposition of the carbon species (impurity) involved intrinsically in TiO_2 (Fig. SI 2). Even considering these results (negative data), TiO_2 effectively exhibited the photocatalytic decomposition of toluene into CO_2 , in particular under blue light irradiation. The photocatalytic decomposition of benzene, m-xylene and methylcyclohexane into CO_2 were also successfully demonstrated on TiO_2 under illumination from the blue and green LED lamps (Fig. SI 3). It is noted that methylcyclohexane, having the same frame structure with toluene, can be also decomposed to CO_2 on TiO_2 under visible light irradiation, although the reaction activity is lower than that of toluene. These results indicate that not only $\text{sp}^2 \text{C}=\text{C}$ but also $\text{sp}^3 \text{C}-\text{C}$ bonds could be activated by visible light. Durability testing for the photocatalytic decomposition of toluene was also performed and the reactivity was found to be maintained even after five repetitions (Fig. SI 4). It was thus confirmed that the photocatalytic decomposition reaction of VOCs successfully proceeded by visible light energies that do not allow bandgap excitation of TiO_2 .

3.2. Visible-light responsive interfacial surface complex (ISC) on the TiO_2

TiO_2 itself is known to show no optical absorption, but Fig. 2 [I] shows absorption observed in the visible light region above 400 nm. There are two possible reasons for this as follows: first, the impurity carbon species may act as a photosensitizer. In fact, it is true that CO_2 was produced in very small amounts when visible-light irradiation of TiO_2 photocatalyst in the absence of VOCs was conducted for a long time, confirming that the carbon source was involved in TiO_2 . The second is that barium sulphate (BaSO_4) was used as a reference for 100% reflectance, which may have affected the relative reflectance of TiO_2 and appeared as background in the visible light region. It is noted that similar absorption spectrum of TiO_2 (P-25, Degussa) was previously observed in the visible light region [50,51]. From these results, it is reasonable to discuss only the change in absorbance before and after VOC adsorption on TiO_2 . When toluene was adsorbed on the TiO_2 , a new

optical absorption was appeared at around 420 to 540 nm in the visible-light region. Fig. 2 [II] shows the difference spectrum which was obtained by subtracting the spectrum of TiO_2 from the toluene-adsorbed TiO_2 . The absorbance observed at 420–540 nm was assigned to the interfacial surface complex (ISC) formed by the interaction between TiO_2 and toluene. Fig. 2 [II] also shows the relationship between the difference absorption spectrum, and energy distribution illuminated from LED lamps. These results show that the surface complexes can absorb visible light (420 to 540 nm) emitted from blue and green lamps, but can hardly absorb light above 600 nm wavelength emitted from the red lamp. In fact, as shown in Fig. 1, the visible light emitted from blue and green LED lamps activate the surface complexes and the photooxidation reaction proceeds, whereas the reactions hardly proceed with the light above 600 nm. Furthermore, interaction of various reactant molecules with the TiO_2 surface exhibited visible light absorption from 420 to 540 nm, which are attributable to ISCs with different absorbance (Fig. SI 5). And the photoexcitation of ISCs may have led to the complete photodegradation of VOC to CO_2 (Table 1). In order to understand the photochemical properties of the ISC, effects of the light irradiation intensity, and the apparent quantum yields for the photocatalytic activities were investigated. Effects of the photo-intensity illuminated from the blue LED lamp on the photocatalytic activities are shown in Fig. SI 6. The photocatalytic activity was seen to depend on light intensity, with higher light intensities increasing the reaction activity, which was almost saturated at light irradiations of 6.8×10^4 lx or higher. Fig. 3 shows the apparent quantum yields (Φ) for the photocatalytic decomposition of toluene on TiO_2 as a function of the photo-irradiation wavelength. The photo-response for the photocatalytic decomposition of toluene was confirmed up to ca. 540 nm and the apparent quantum yields were estimated to be 1.06% under photo-irradiation at 510 nm, 2.38% at 450 nm, and 3.53% at 420 nm. It was observed that a good correlation was obtained between the photocatalytic activity and the absorbance of the ISC at each light wavelength. These results indicate that the visible light absorption of ISC plays an important role in the photocatalytic reaction.

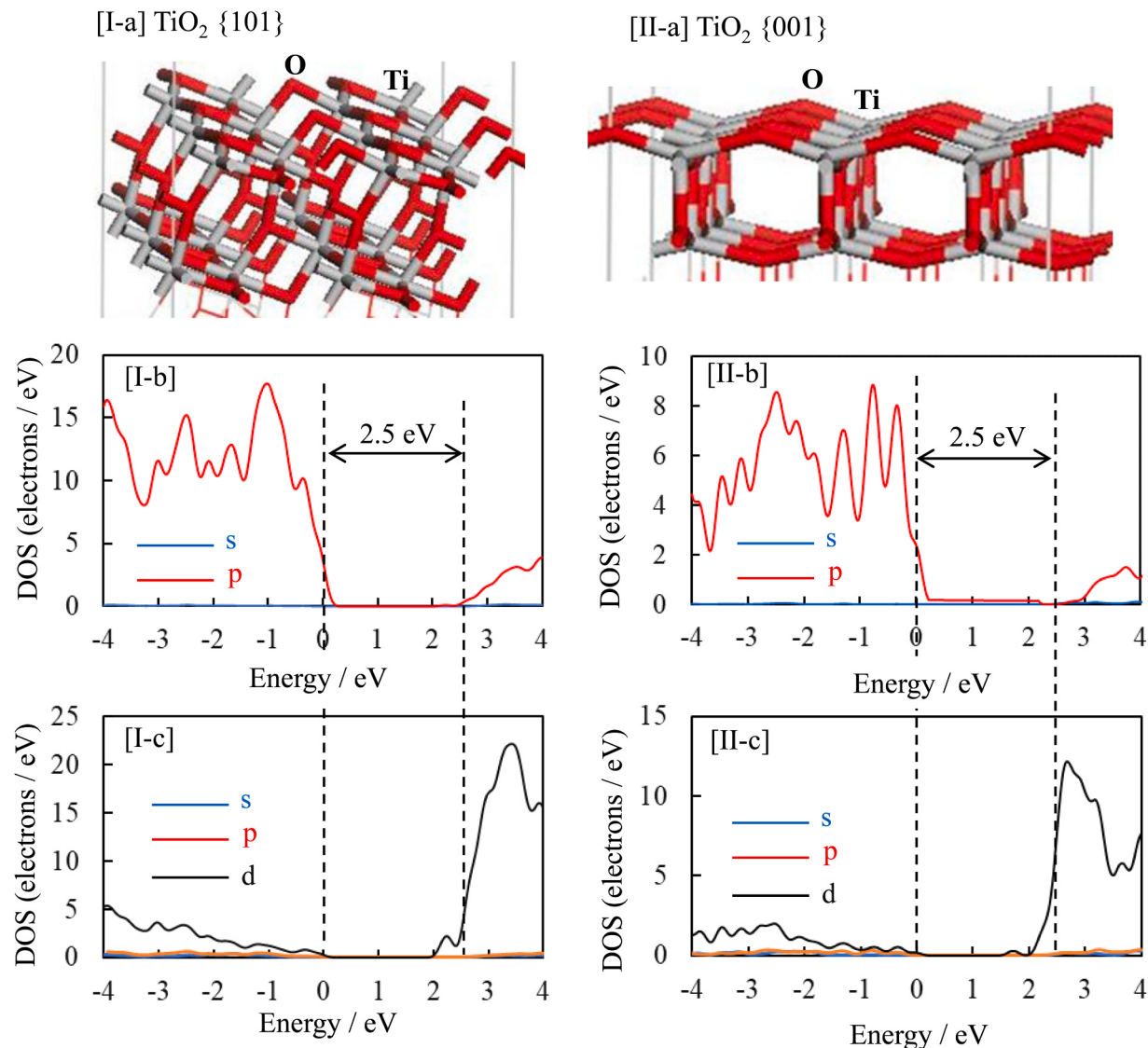


Fig. 4. Atomic surface structures of [I-a] TiO_2 {101} and [II-a] TiO_2 {001} facets and their projected density of states (PDOS) of (I, II-b) O, (I, II-c) Ti.

3.3. Identification of the ISC as the active sites for photocatalysis

In our previous study, the interaction of the surface Ti-OH species with benzyl alcohol was critical for the selective photocatalytic oxidation of benzyl alcohol to benzaldehyde [52,53]. To investigate the effect of the surface Ti-OH on the photocatalytic activity for toluene decomposition, TiO_2 was treated with dilute hydrofluoric acid solution to form HF-TiO₂. XPS analysis showed that HF(110)-TiO₂ exhibited an XPS peak at ~ 685 eV due to F1s which were assigned to $\equiv\text{Ti}-\text{F}$ as a result of OH substitution on the surface of TiO_2 (Fig. SI 7) [54]. The HF(110)-TiO₂ and TiO_2 itself showed almost the same activity for the decomposition of toluene to CO₂ (Fig. SI 8). That is, it was clearly seen that the surface Ti-OH species hardly participated in the photocatalytic decomposition of toluene under visible-light irradiation.

Various kinds of commercial TiO_2 photocatalysts were tested for the photocatalytic decomposition of acetic acid into CO₂, and the relationship between the surface area of TiO_2 and the photocatalytic activity was examined (Fig. SI 9). The photocatalytic activity increased as the surface area of TiO_2 increased. For example, the photocatalytic activity on ST-01 was observed to be higher than that on P-25 photocatalyst. It was also confirmed that anatase type TiO_2 was more active when comparing anatase or rutile type TiO_2 with the same surface area.

According to XRD analysis, it was confirmed that TiO_2 photocatalysts for JRC-TIO 7–13 have an anatase structure (PDF no. 21-1272), for JRC-TIO-6 with a rutile structure (PDF no. 21-127) and P-25 (a mixture of anatase and rutile) (Fig. SI 10). The (200) and (004) peaks indicate that the crystal grows towards the {001} facet [55]. From the analysis of XRD patterns of various TiO_2 photocatalysts, the ratio of {001} facet was roughly estimated to be ca. 20–28% in the crystal phase (Fig. SI 11). It was observed that more {001} facets are exposed in P-25 than in ST-01 photocatalyst. The photocatalytic activity per unit surface area as a function of the ratio of {001} facet exposed was shown in Fig. SI 12. The reaction activity per unit surface area of TiO_2 was observed to be higher for P-25 than for ST-01. This reaction activity was found to be related to the degree of the {001} facet exposure, suggesting that the more {001} facets exposed, the higher the reaction activity.

In order to understand the effect of TiO_2 crystal facets on the surface activity in detail, DFT simulations on the {001} and {101} facets of TiO_2 were performed. The atomic surface structures of the anatase TiO_2 {101} and {001} facets are shown in Fig. 4 [I-a and II-a], respectively. The {001} facets are expected to have higher surface activity than the {101} facets because the Ti-O-Ti bond angle is larger and the surface energy higher. Fig. 4 [I-b, c and II-b, c] shows the projected density of states (PDOS) of O and Ti for the {101} and {001} facets of the TiO_2

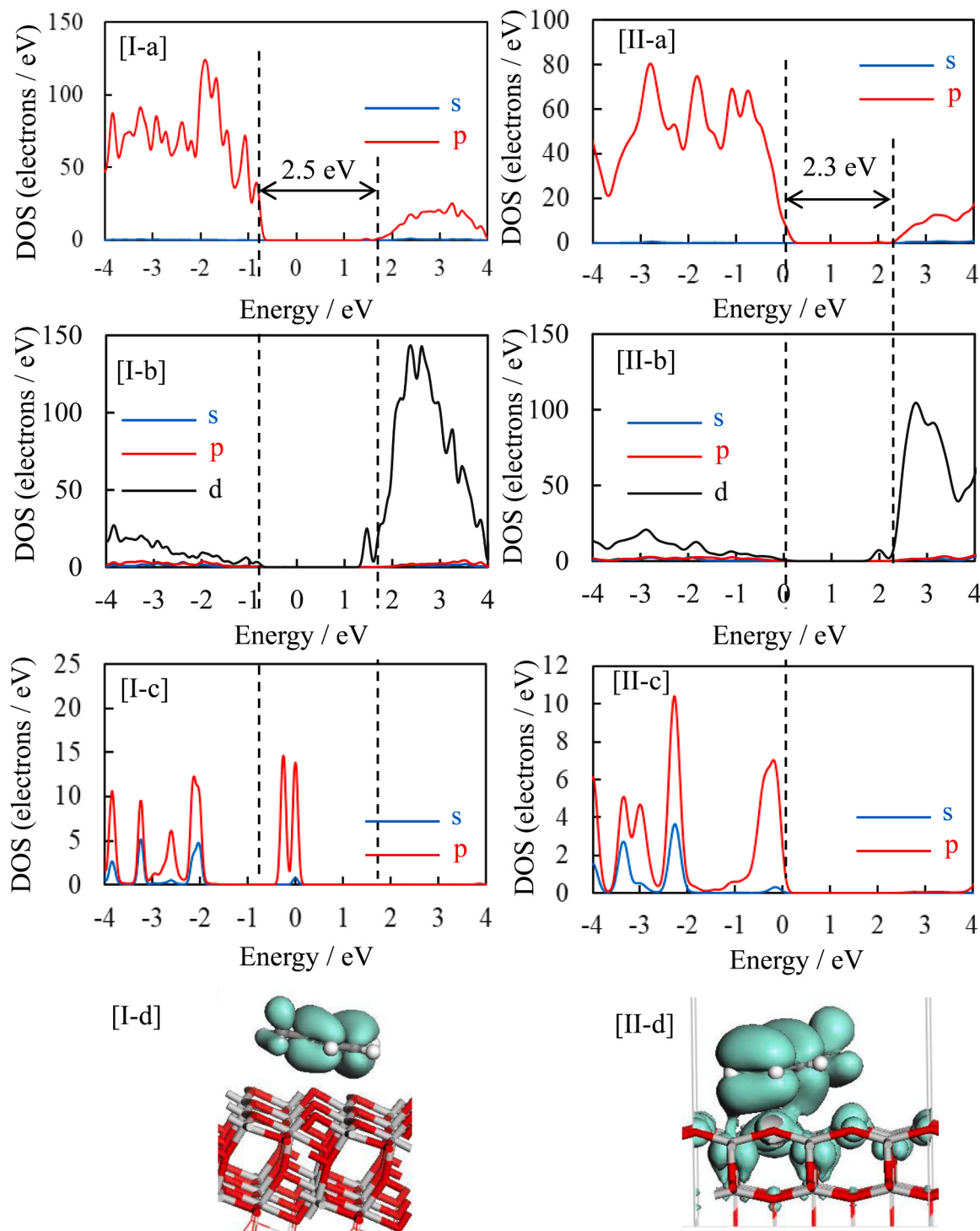


Fig. 5. Projected density of states (PDOS) of (a) O, (b) Ti, (c) C; and (d) electron density contour map of HOMOs for [I] the toluene-adsorbed TiO₂ {101} and [II] toluene-adsorbed TiO₂ {001}, respectively.

surface, respectively. The valence band maximum (VBM) and conduction band minimum (CBM) of TiO₂ mainly consist of O 2p and Ti 3d orbitals, respectively. The bandgaps of the TiO₂ {101} and {001} facets were ca. 2.5 eV which is considerably smaller than the experimental value of 3.2 eV (380 nm). Two reasons are conceived: (i) error in the common density functionals, and/or (ii) slab models were used rather than the bulk. However, in this study, we focused on the different interactions of toluene with the {101} and {001} facets of the TiO₂ slabs.

The state of adsorption of toluene on the TiO₂ surface has been optimized. As a result, the benzene ring of toluene approached the TiO₂

{101} and {001} in a parallel plane. The adsorption stability of toluene on these slabs were examined and it was found that the adsorption energy on the {001} facet was larger by 0.5 eV than that on {101}, suggesting that toluene strongly interacted with the {001} facet of TiO₂. In fact, the distance between the TiO₂ surface and toluene was shorter for TiO₂ {001} than for {101} (Fig. SI 13). Fig. 5 [I-a-c] shows the PDOS of O, Ti and C after adsorption of toluene on the {101} facet of TiO₂. The bandgap of TiO₂{101} interacting with toluene remained unchanged at ca. 2.5 eV. The orbital hybridization of toluene with TiO₂ was not observed, and the C 2p π orbitals alone of toluene was located above the

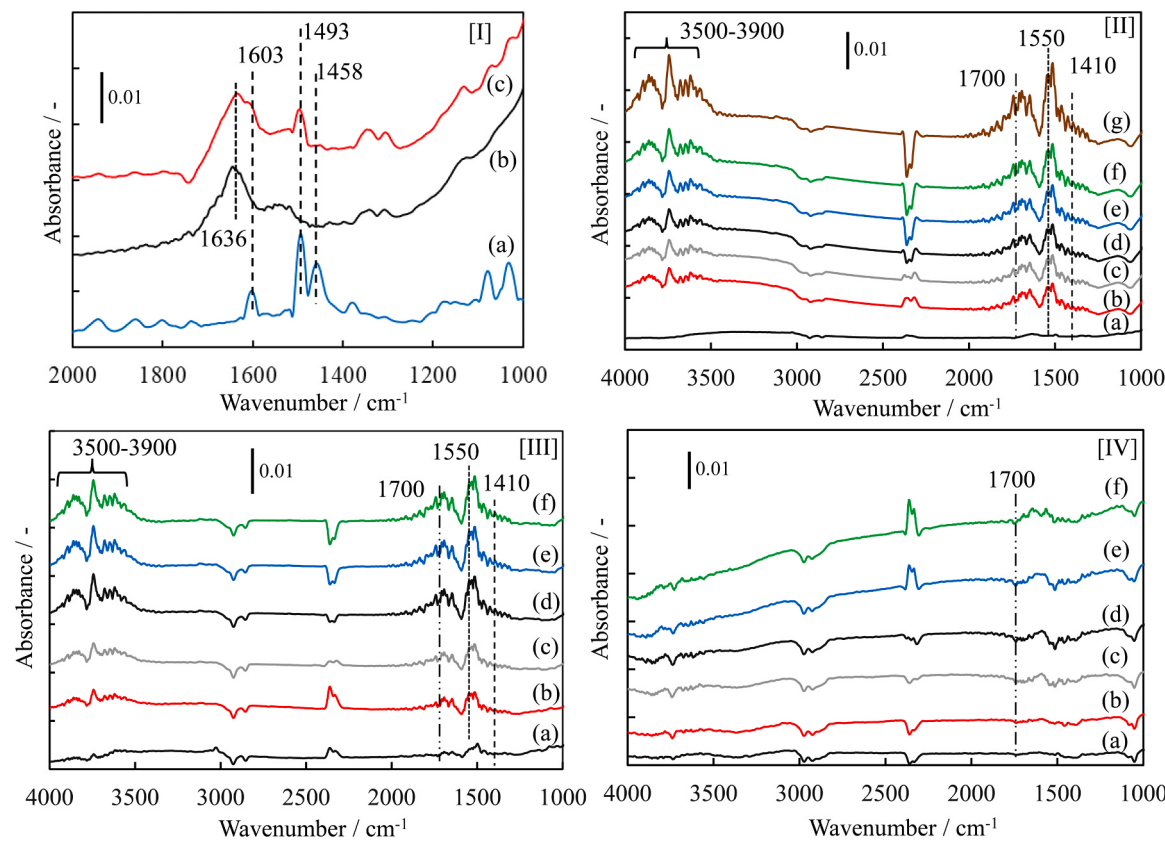


Fig. 6. ATR FT-IR spectra of [I] (a) toluene itself, (b) TiO_2 itself, and (c) TiO_2 -adsorbed toluene before illumination. Changes in the ATR FT-IR spectra of the TiO_2 -adsorbed toluene after photo-irradiation from [II] blue, [III] green, and [IV] red LED lamps for (a) 0, (b) 1, (c) 5, (d) 15, (e) 30 and (f) 40 and (g) 120 min.

VBM of TiO_2 , forming the highest occupied molecular orbitals (HOMO) (Fig. 5 I-d). On the other hand, Fig. 5 [II-a-c] shows the PDOS of O, Ti and C after adsorption of toluene on the TiO_2 {001} facet. The bandgap was observed to decrease from ca. 2.5 eV before adsorption to ca. 2.3 eV after adsorption. The band-narrowing (formation of the subband) is attributed to the ISC formed by orbital hybridization between the π orbitals of toluene and the O 2p orbitals on the TiO_2 {001} facet, i.e., σ bonds formed by the interaction between the C 2p in the aromatic π orbital in toluene and the O 2p in TiO_2 constructed the HOMO (Fig. 5 II-d). On the other hand, the LUMO was composed of Ti 3d orbitals of TiO_2 . Therefore, ISC was assumed to be photo-excited at energies smaller than

the band gap of TiO_2 , resulting in electron transfer from the HOMO to the LUMO. The photo-excitation of the ISC through the ligand to metal charge transfer (LMCT) could consider to induce charge separation, initiating the photocatalytic reactions.

To understand the difference in mixing orbitals between toluene and the TiO_2 facets, the work functions of the {101} and {001} slabs of TiO_2 were further investigated and estimated to be 6.19 and 5.39 eV, respectively (Fig. S1 14). The work functions of the single crystal TiO_2 {101} and {001} were previously reported experimentally to be 3.92 eV and 3.84 eV, respectively, in 0.5 M KCl solution [56]. Although the values calculated were less quantitative, the VBM on the {101} facet was confirmed to have a deeper potential than for {001}. The VBM for the {001} slab seemed to match the energy level for the π orbital of toluene, leading to a hybridization of orbitals and formation of the subband above the valence band. DFT calculations were, thus, performed to understand the interactions between aromatic hydrocarbons and TiO_2 {001} in order to clarify its potential for visible light response. The important visible-light-responsive active sites in this reaction system are, thus, considered to be the ISCs formed from the VOCs adsorbed on the TiO_2 {001} facet. They were revealed by UV-Visible light absorption spectra, apparent quantum yields and DFT calculations.

3.4. Understanding the reaction mechanism for the photocatalytic decomposition of toluene

To check the adsorption state of toluene molecules on TiO_2 , the FT-IR spectra of toluene-adsorbed TiO_2 were investigated (See Fig. 6 [I]). When toluene was adsorbed on TiO_2 , the characteristic IR bands were observed at 1636, 1603, 1493 and 1458 cm^{-1} . The band at 1636 cm^{-1} is attributed to a bending mode of water adsorbed on TiO_2 , while those at 1603, 1493 and 1458 cm^{-1} are due to vibrations of the C=C stretch in the benzene ring [57]. Furthermore, when the toluene-adsorbed TiO_2

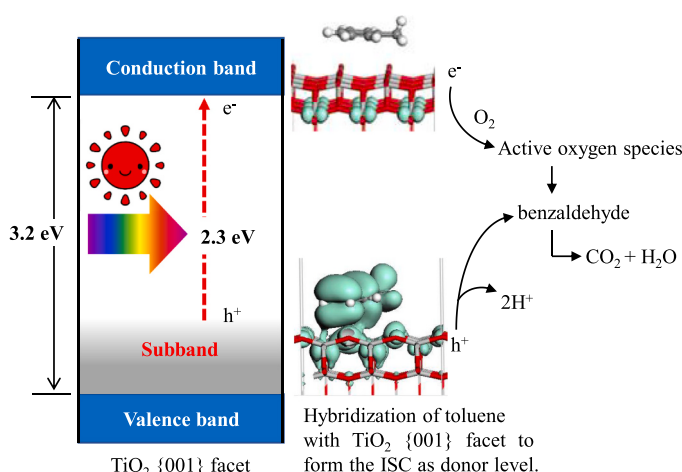


Fig. 7. Mechanisms for the visible-light induced charge separation on TiO_2 by the formation of ISC for the decomposition of toluene.

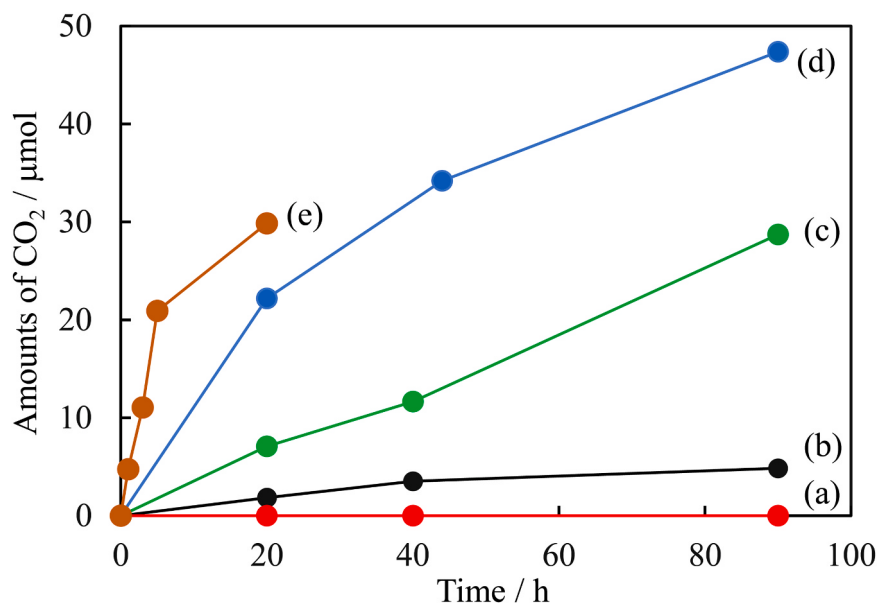


Fig. 8. Thermal effects on the photocatalytic activities for the decomposition of toluene into CO_2 under non-illumination at (a) 353 K, and visible-light irradiation at (b) 278 K, (c) 313 K, (d) 353 K and (e) 393 K. 1.0 μL of toluene was added into the reaction cell.

photocatalysts were photo-irradiated with the blue LED light, the spectra showed an increase in peak intensity at 3500–3900, 1700, 1550 and 1410 cm^{-1} with an increase in the photo-irradiation time (Fig. 6 [II]). The peak at 3500–3900 cm^{-1} was assigned to adsorbed water on the TiO_2 surface [54], the peak at 1700 cm^{-1} to -CHO (formyl group) [58], and the peaks at 1550 and 1410 cm^{-1} to carbonate ions [57]. Similar IR changes were observed with an increase of photo-irradiation from the green lamp (Fig. 6 [III]). On the other hand, when irradiated from a red lamp, benzaldehyde could hardly be formed on the TiO_2 (Fig. 6 [IV]). In fact, after the reaction under blue light irradiation, the adsorbed species extracted from the photocatalyst with acetonitrile was identified to benzaldehyde by HPLC measurement. These results indicate that benzaldehyde as the intermediate species was formed on the TiO_2 surface when toluene-adsorbed TiO_2 was irradiated with the blue light. The results of photoirradiation of methylcyclohexane adsorbed on TiO_2 are also shown in Fig. SI 15. The peaks at 3500–3900, 1700, 1550 and 1410 cm^{-1} significantly increased with an increase in the photo-irradiation time. It was, thus, confirmed that aliphatic compounds such as methyl cyclohexane were also activated under visible light irradiation on TiO_2 to form intermediates with formyl groups.

Fig. 7 shows a proposed reaction mechanism for the photocatalytic decomposition of toluene on TiO_2 under visible light irradiation. The direct bandgap excitation of TiO_2 are known to require UV-light ($h\nu > 3.2 \text{ eV}$). However, when toluene was adsorbed on TiO_2 , the hybridization of toluene with the TiO_2 {001} surface formed an ISC. That is, the ISC itself was photo-oxidized by holes to produce benzaldehyde, while active oxygen species are assumed to form by the multi-electron reduction of O_2 . The active oxygen species subsequently induced deep oxidation of benzaldehyde into CO_2 .

3.5. Thermal effect on the photocatalytic decomposition of toluene to CO_2

Photocatalytic experiments are usually performed at room temperature or under temperature-controlled conditions. Therefore, the local thermal effects induced by visible or infrared light irradiation are often ignored. Since photocatalytic efficiency can generally be improved with the assistance of external or internal thermal energy, "photo-thermo catalysis" is an emerging technique deserving more extensive research [59–61].

Fig. 8 shows the thermal effect in the photocatalytic decomposition

of toluene to CO_2 over a TiO_2 photocatalyst at each temperature (278 ~ 393 K) under blue light irradiation. The photocatalytic activity was appeared at 278 K, but its activity was low. When the reaction temperature was raised, the activity was significantly improved. Although CO_2 was not produced on TiO_2 by the thermal reaction of toluene at 353 K under dark conditions, the synergistic effect of light and heat dramatically improved the photocatalytic activity. It was, thus, observed that when the heat generated from the LEDs was successfully collected and used as thermal energy to raise the temperature, the reaction activity increased dramatically. At 393 K, the initial activity of the reaction was high, while the total amounts of CO_2 significantly decreased. This is probably because the amounts of adsorbed molecules on TiO_2 decreased at higher temperature. When considering the photocatalyst as a zero-order reaction, the activation energy was estimated to be 27.1 kJ/mol (Fig. SI 16). The activation energy can be attributed to the transportation efficiency of the charge carriers generated on the semiconductor photocatalyst. The supply of thermal energy is, thus, important to improve the activity of the visible light responsive TiO_2 photocatalyst.

4. Conclusions

It was clearly demonstrated that TiO_2 is able to exhibit the photocatalytic decomposition of various VOCs into CO_2 under visible-light irradiation. In particular, VOCs such as benzene, toluene and m-xylene (BTX) were effectively decomposed into CO_2 under visible-light (2.3 eV $< h\nu$). This is because the toluene-adsorbed TiO_2 exhibited visible-light absorption due to the interfacial surface complexes (ISC). By density functional theory (DFT) calculations, it was confirmed that the ISC exists as donor levels above the valence band of the TiO_2 by hybridization between O 2p in TiO_2 and C 2p in toluene, which caused the apparent narrowing of the TiO_2 bandgap. The charge separation in the ISC through the ligand to metal charge transfer (LMCT) by visible-light irradiation consider to induce the photocatalytic reactions. FT-IR measurements revealed that the initial photo-oxidation of toluene to benzaldehyde on the TiO_2 surface was triggered by the activation of the ISC under visible light irradiation, followed by further deep oxidation of benzaldehyde into CO_2 . Moreover, the combination of photo-energy and thermal-energy induced photo-thermal TiO_2 catalysis, promoting the complete decomposition reaction of toluene into CO_2 . The findings

provided fundamental insights into the effect of the interaction between the TiO₂ surface and the reactant molecules, opening up new strategies for the development of visible light-responsive photocatalysts for environmental remediation and the effective utility of visible light and excess heat promote reaction activity.

CRediT authorship contribution statement

Imai Kousuke: Investigation, Methodology, Writing – original draft.
Fukushima Takashi: Writing – review & editing.
Kobayashi Hisayoshi: Investigation, Methodology, Writing – review & editing.
Higashimoto Shinya: Conceptualization, Methodology, Supervision, Writing – review & editing.

Declaration of Competing Interest

The authors declare that they have no known competing financial interests or personal relationships that could have appeared to influence the work reported in this paper.

Data availability

Data will be made available on request.

Appendix A. Supporting information

Supplementary data associated with this article can be found in the online version at [doi:10.1016/j.apcatb.2024.123745](https://doi.org/10.1016/j.apcatb.2024.123745).

References

- [1] X. Chen, S. Mao, Titanium dioxide nanomaterials: synthesis, properties, modifications, and applications, *Chem. Rev.* 197 (2007) 2891–2959, <https://doi.org/10.1021/cr0500535>.
- [2] J. Schneider, M. Matsuoka, M. Takeuchi, J. Zhang, Y. Horiuchi, M. Anpo, D. W. Bahnemann, Understanding TiO₂ photocatalysis: mechanisms and materials, *Chem. Rev.* 114 (2014) 9919–9986, <https://doi.org/10.1021/cr5001892>.
- [3] Y. Ma, X. Wang, Y. Jia, X. Chen, H. Han, C. Li, Titanium dioxide-based nanomaterials for photocatalytic fuel generations, *Chem. Rev.* 114 (2014) 9987–10043, <https://doi.org/10.1021/cr500008u>.
- [4] J. Kou, C. Lu, J. Wang, Y. Chen, Z. Xu, R.S. Varma, Selectivity enhancement in heterogeneous photocatalytic transformations, *Chem. Rev.* 117 (2017) 1445–1514, <https://doi.org/10.1021/acs.chemrev.6b00396>.
- [5] H. Yamashita, K. Mori, Y. Kuwahara, T. Kamegawa, M. Wen, P. Verma, M. Che, Single-site and nano-confined photocatalysts designed in porous materials for environmental uses and solar fuels, *Chem. Soc. Rev.* 47 (2018) 8072–8096, <https://doi.org/10.1039/C8CS00341F>.
- [6] S. Higashimoto, Titanium dioxide-based visible-light sensitive photocatalysis: mechanistic insight and applications, *Catalysts* 9 (2019) 201, <https://doi.org/10.3390/catal9020201>.
- [7] H. Einaga, S. Futamura, T. Ibusuki, Heterogeneous photocatalytic oxidation of benzene, toluene, cyclohexene and cyclohexane in humidified air: comparison of decomposition behavior on photoirradiated TiO₂ catalyst, *Appl. Catal. B Environ.* 38 (2002) 215–225, [https://doi.org/10.1016/S0926-3373\(02\)00056-5](https://doi.org/10.1016/S0926-3373(02)00056-5).
- [8] A. Bouaza, A. Laplanche, Photocatalytic degradation of toluene in the gas phase: comparative study of some TiO₂ supports, *J. Photochem. Photobiol. A* 150 (2002) 207–212, [https://doi.org/10.1016/S1010-6030\(02\)00088-6](https://doi.org/10.1016/S1010-6030(02)00088-6).
- [9] Z. Pengyi, L. Juan, Z. Zhongliang, VUV photocatalytic degradation of toluene in the gas phase, *Chem. Lett.* 33 (2004) 1242–1243, <https://doi.org/10.1246/cl.2004.1242>.
- [10] Y. Luo, W.S. Tai, H.O. Seo, K.-D. Kim, M.J. Kim, N.K. Dey, Y.D. Kim, K.H. Choi, D. C. Lim, Adsorption and photocatalytic decomposition of toluene on TiO₂ surfaces, *Catal. Lett.* 138 (2010) 76–81, <https://doi.org/10.1007/s10562-010-0369-1>.
- [11] Y. Shen, S. Liu, L. Lu, C. Zhu, Q. Fang, R. Liu, Z. He, Y. Li, S. Song, Photocatalytic degradation of toluene by a TiO₂ p-n homojunction nanostructure, *ACS Appl. Nano Mater.* 5 (2022) 18612–18621, <https://doi.org/10.1021/acsnm.2c04397>.
- [12] J. Zhang, P. Zhou, J. Liu, J. Yu, New understanding of the difference of photocatalytic activity among anatase, rutile and brookite TiO₂, *Phys. Chem. Chem. Phys.* 16 (2014) 20382–20386, <https://doi.org/10.1039/C4CP02201G>.
- [13] G. Žerjav, K. Žízek, J. Zavašnik, A. Pintar, Brookite vs. rutile vs. anatase: what's behind their various photocatalytic activities? *J. Environ. Chem. Eng.* 10 (3) (2022) 107722 <https://doi.org/10.1016/j.jece.2022.107722>.
- [14] K. Fischer, A. Gawel, D. Rosen, M. Krause, A.A. Latif, J. Griebel, A. Prager, A. Schulze, Low-temperature synthesis of anatase/rutile/brookite TiO₂ nanoparticles on a polymer membrane for photocatalysis, *Catalysts* 7 (2017) 209, <https://doi.org/10.3390/catal7070209>.
- [15] M. Bellardita, A.D. Paola, B. Megna, L. Palmisano, Absolute crystallinity and photocatalytic activity of brookite TiO₂ samples, *Appl. Catal. B Environ.* 201 (2017) 150–158, <https://doi.org/10.1016/j.apcatb.2016.08.012>.
- [16] M. Bellardita, A.D. Paola, B. Megna, L. Palmisano, Determination of the crystallinity of TiO₂ photocatalysts, *J. Photochem. Photobio. A Chem.* 367 (2018) 312–320, <https://doi.org/10.1016/j.jphotochem.2018.08.042>.
- [17] K. Nakata, A. Fujishima, TiO₂ photocatalysis: design and applications, *J. Photochem. Photobio. C Photochem. Rev.* 13 (3) (2012) 69–189, <https://doi.org/10.1016/j.jphotochemrev.2012.06.001>.
- [18] T. Tachikawa, S. Yamashita, T. Majima, Evidence for crystal-face-dependent TiO₂ photocatalysis from single-molecule imaging and kinetic analysis, *J. Am. Chem. Soc.* 133 (18) (2011) 7197–7204, <https://doi.org/10.1021/ja201415j>.
- [19] N. Wu, J. Wang, D.N. Tafen, H. Wang, J.-G. Zheng, J.P. Lewis, X. Liu, S.S. Leonard, A. Manivannan, Shape-enhanced photocatalytic activity of single-crystalline anatase TiO₂ (101) nanobelts, *J. Am. Chem. Soc.* 132 (19) (2010) 6679–6685, <https://doi.org/10.1021/ja909456f>.
- [20] C. Retamoso, N. Escalona, M. González, L. Barrientos, P. Allende-González, S. Stancovich, R. Serpell, J.L.G. Fierro, M. Lopez, Effect of particle size on the photocatalytic activity of modified rutile sand (TiO₂) for the discoloration of methylene blue in water, *J. Photochem. Photobiol. A Chem.* 378 (2019) 136–141, <https://doi.org/10.1016/j.jphotochem.2019.04.021>.
- [21] H.D. Jang, S.K. Kim, S.J. Kim, Effect of particle size and phase composition of titanium dioxide nanoparticles on the photocatalytic properties, *J. Nanopart. Res.* 3 (2001) 141–147, <https://doi.org/10.1023/A:1017948330363>.
- [22] L. Gao, Q. Zhang, Effects of amorphous contents and particle size on the photocatalytic properties of TiO₂ nanoparticles, *Scr. Mater.* 44 (8–9) (2001) 1195–1198, [https://doi.org/10.1016/S1359-6462\(01\)00681-9](https://doi.org/10.1016/S1359-6462(01)00681-9).
- [23] K.L. Yeung, S.T. Yau, A.J. Maira, J.M. Coronado, J. Soria, P.L. Yue, The influence of surface properties on the photocatalytic activity of nanostructured TiO₂, *J. Catal.* 219 (2003) 107–116, [https://doi.org/10.1016/S0021-9517\(03\)00187-8](https://doi.org/10.1016/S0021-9517(03)00187-8).
- [24] X. Pan, M.-Q. Yang, X. Fu, N. Zhang, Y.-J. Xu, Defective TiO₂ with oxygen vacancies: synthesis, properties and photocatalytic applications, *Nanoscale* 5 (2013) 3601–3614, <https://doi.org/10.1039/C3NR00476G>.
- [25] D. Ariyanti, L. Mills, J. Dong, Y. Yao, W. Gao, NaBH₄ modified TiO₂: defect site enhancement related to its photocatalytic activity, *Mater. Chem. Phys.* 199 (2017) 571–576, <https://doi.org/10.1016/j.matchemphys.2017.07.054>.
- [26] H. Zhao, F. Pan, Y. Li, A review on the effects of TiO₂ surface point defects on CO₂ photoreduction with H₂O, *J. Mater.* 3 (2017) 17–32, <https://doi.org/10.1016/j.jmat.2016.12.001>.
- [27] H. Wang, Q. Chen, Q. Luan, R. Duan, R. Guan, X. Cao, X. Hu, Photocatalytic properties dependent on the interfacial defects of intergrains within TiO₂ mesocrystals, *Chem. Eur. J.* 24 (2018) 17105–17116, <https://doi.org/10.1002/chem.201803516>.
- [28] J. Zhu, J. Wang, F. Lv, S. Xiao, C. Nuckolls, H. Li, Synthesis and self-assembly of photonic materials from nanocrystalline titania sheets, *J. Am. Chem. Soc.* 135 (2013) 4719–4721, <https://doi.org/10.1021/ja401334j>.
- [29] J. Yu, J. Low, W. Xiao, P. Zhou, M. Jaroniec, Enhanced photocatalytic CO₂-reduction activity of anatase TiO₂ by coexposed {001} and {101} facets, *J. Am. Chem. Soc.* 136 (25) (2014) 8839–8842, <https://doi.org/10.1021/ja5044787>.
- [30] H. Tang, Z. Cheng, S. Dong, X. Cui, H. Feng, X. Ma, B. Luo, A. Zhao, J. Zhao, B. Wang, Understanding the intrinsic chemical activity of anatase TiO₂ (001)-(1×4) surface, *J. Phys. Chem. C* 121 (2017) 1272–1282, <https://doi.org/10.1021/acs.jpcc.6b12917>.
- [31] H.G. Yang, C.H. Sun, S.Z. Qiao, J. Zou, G. Liu, S.C. Smith, H.M. Cheng, G.Q. Lu, Anatase TiO₂ single crystals with a large percentage of reactive facets, *Nature* 453 (2008) 638–641, <https://doi.org/10.1038/nature06964>.
- [32] X. Han, X. Wang, S. Xie, Q. Kuang, J. Ouyang, Z. Xie, L. Zheng, Carbonate ions-assisted syntheses of anatase TiO₂ nanoparticles exposed with high energy (001) facets, *RSC Adv.* 2 (2012) 3251–3253, <https://doi.org/10.1039/C2RA00834C>.
- [33] H.G. Yang, G. Liu, S.Z. Qiao, C.H. Sun, Y.G. Jin, S.C. Smith, J. Zou, H.M. Cheng, G. Q. Lu, Solvothermal synthesis and photoreactivity of anatase TiO₂ nanosheets with dominant {001} facets, *J. Am. Chem. Soc.* 131 (2009) 4078–4083, <https://doi.org/10.1021/ja808790p>.
- [34] X. Han, Q. Kuang, M. Jin, Z. Xie, L. Zheng, Synthesis of titania nanosheets with a high percentage of exposed (001) facets and related photocatalytic properties, *J. Am. Chem. Soc.* 131 (2009) 3152–3153, <https://doi.org/10.1021/ja8092373>.
- [35] R. Asahi, T. Morikawa, K. Aoki, Y. Taga, Visible-light photocatalysis in nitrogen-doped titanium oxides, *Science* 293 (2001) 269–271, <https://doi.org/10.1126/science.1061051>.
- [36] R. Asahi, T. Morikawa, H. Irie, T. Ohwaki, Nitrogen-doped titanium dioxide as visible light-sensitive photocatalyst: designs, developments, and prospects, *Chem. Rev.* 114 (2014) 9824–9852, <https://doi.org/10.1021/cr5000738>.
- [37] S. Higashimoto, Y. Ushiroda, M. Azuma, H. Ohue, Synthesis, characterization and photocatalytic activity of N-doped TiO₂ modified by platinum chloride, *Catal. Today* 122 (2008) 165–169, <https://doi.org/10.1016/j.cattod.2008.01.014>.
- [38] S. Higashimoto, W. Tanihata, Y. Nakagawa, M. Azuma, H. Ohue, Y. Sakata, Effective photocatalytic decomposition of VOC under visible-light irradiation on N-doped TiO₂ modified with vanadium species, *Appl. Catal. A Gen.* 340 (2008) 98–104, <https://doi.org/10.1016/j.apcata.2008.02.003>.
- [39] S. Higashimoto, T. Nishi, M. Yasukawa, M. Azuma, Y. Sakata, H. Kobayashi, Photocatalysis of titanium dioxide modified by catechol-type interfacial surface complexes (ISC) with different substituted groups, *J. Catal.* 329 (2015) 286–290, <https://doi.org/10.1016/j.jcat.2015.05.010>.
- [40] S. Higashimoto, N. Kitao, N. Yoshida, T. Sakura, M. Azuma, H. Ohue, Y. Sakata, Selective photocatalytic oxidation of benzyl alcohol and its derivatives into corresponding aldehydes by molecular oxygen on titanium dioxide under visible

- light irradiation, *J. Catal.* 266 (2009) 279–285, <https://doi.org/10.1016/j.jcat.2009.06.018>.
- [41] S. Higashimoto, N. Suetsugu, M. Azuma, H. Ohue, Y. Sakata, Efficient and selective oxidation of benzyl alcohol by O₂ into corresponding aldehydes on a TiO₂ photocatalyst under visible light irradiation: Effect of phenyl-ring substitution on the photocatalytic activity, *J. Catal.* 274 (2010) 76–83, <https://doi.org/10.1016/j.jcat.2010.06.006>.
- [42] H. Kobayashi, S. Higashimoto, DFT study on the reaction mechanisms behind the catalytic oxidation of benzyl alcohol into benzaldehyde by O₂ over anatase TiO₂ surfaces with hydroxyl groups: role of visible-light irradiation, *Appl. Catal. B Environ.* 170 (2015) 135–143, <https://doi.org/10.1016/j.apcatb.2015.01.035>.
- [43] H. Ariga, T. Taniike, H. Morikawa, M. Tada, B.K. Min, K. Watanabe, Y. Matsumoto, S. Ikeda, K. Saiki, Y. Iwasawa, Surface-mediated visible-light photo-oxidation on Pure TiO₂(001), *J. Am. Chem. Soc.* 131 (41) (2009) 14670–14672, <https://doi.org/10.1021/ja9066805>.
- [44] L. Ren, Y. Li, J. Hou, J. Bai, M. Mao, M. Zeng, X. Zhao, N. Li, The pivotal effect of the interaction between reactant and anatase TiO₂ nanosheets with exposed {001} facets on photocatalysis for the photocatalytic purification of VOCs, *Appl. Catal. B Environ.* 181 (2016) 625–634, <https://doi.org/10.1016/j.apcatb.2015.08.034>.
- [45] S.J. Clark, M.D. Segall, C.J. Pickard, P.J. Hasnip, M.J. Probert, K. Refsen, M. C. Payne, First principles methods using CASTEP, *Z. fuer Krist.* 220 (2005) 567–570.
- [46] J.P. Perdew, K. Burke, M. Ernzerhof, Generalized gradient approximation made simple. [Erratum to document cited in CA126:51093, Phys. Rev. Lett. 78 (1997) 1396, <https://doi.org/10.1103/PhysRevLett.78.1396>.]
- [47] K. Laasonen, R. Car, C. Lee, D. Vanderbilt, Implementation of ultrasoft pseudopotentials in ab initio molecular dynamics, *Phys. Rev. B* 43 (1991) 6796–6799, <https://doi.org/10.1103/PhysRevB.43.6796>.
- [48] D.R. Hamann, Generalized norm-conserving pseudopotentials, *Phys. Rev. B* 40 (1989) 2980, <https://doi.org/10.1103/PhysRevB.40.2980>.
- [49] E.R. McNellis, J. Meyer, K. Reuter, Azobenzene at coinage metal surfaces: role of dispersive van der Waals interactions, *Phys. Rev. B* 80 (2009) 205414, <https://doi.org/10.1103/PhysRevB.80.205414>.
- [50] N.P. Xekoukoulotakis, D. Mantzavinos, R. Dillert, D. Bahnemann, Synthesis and photocatalytic activity of boron-doped TiO₂ in aqueous suspensions under UV-A irradiation, *Water Sci. Technol.* 61 (10) (2010) 2501–2506, <https://doi.org/10.2166/wst.2010.150>.
- [51] Z. Duan, Y. Huang, D. Zhang, S. Chen, Electrospinning fabricating Au/TiO₂ network-like nanofibers as visible light activated photocatalyst, *Sci. Rep.* 9 (2019) 8008, <https://doi.org/10.1038/s41598-019-44422-w>.
- [52] S. Higashimoto, K. Okada, T. Morisugi, M. Azuma, H. Ohue, T.-H. Kim, M. Matsuoka, M. Anpo, Effect of Surface treatment on the selective photocatalytic oxidation of benzyl alcohol into benzaldehyde by O₂ on TiO₂ under visible light, *Top. Catal.* 53 (2010) 578–583, <https://doi.org/10.1007/s11244-010-9490-z>.
- [53] S. Higashimoto, K. Okada, M. Azuma, H. Ohue, T. Terai, Y. Sakata, Characteristics of the charge transfer surface complex on titanium(iv) dioxide for the visible light induced chemo-selective oxidation of benzyl alcohol, *RSC Adv.* 2 (2012) 669–676, <https://doi.org/10.1039/C1RA00417D>.
- [54] Y. Yang, K. Ye, D. Cao, P. Gao, M. Qiu, L. Liu, P. Yang, Efficient charge separation from F⁻ Selective Etching and Doping of Anatase-TiO₂{001} for enhanced photocatalytic hydrogen production, *ACS Appl. Mater. Interfaces* 10 (2018) 19633–19638, <https://doi.org/10.1021/acsami.8b02804>.
- [55] H.G. Yang, C.H. Sun, S.Z. Qiao, J. Zou, G. Liu, S.C. Smith, H.M. Cheng, G.Q. Lu, Anatase TiO₂ single crystals with a large percentage of reactive facets, *Nature* 453 (2008) 638–641, <https://doi.org/10.1038/nature06964>.
- [56] V. Mansfeldova, M. Zlamalova, H. Tarabkova, P. Janda, M. Vorokhta, L. Pilial, L. Kavan, Work function of TiO₂ (anatase, rutile, and brookite) single crystals: effects of the environment, *J. Phys. Chem. C* 125 (3) (2021) 1902–1912, <https://doi.org/10.1021/acs.jpcc.0c10519>.
- [57] G. Martra, Lewis acid and base sites at the surface of microcrystalline TiO₂ anatase: relationships between surface morphology and chemical behaviour, *Appl. Catal. A Gen.* 200 (2000) 275–285, [https://doi.org/10.1016/S0926-860X\(00\)00641-4](https://doi.org/10.1016/S0926-860X(00)00641-4).
- [58] R.M. Silverstein, G.C. Bassler, T.C. Morrill, *Spectrometric Identification of Organic Compounds*, fifth ed., John Wiley & Sons, Hoboken, 1991.
- [59] D. Mateo, J.L. Cerrillo, S. Durini, J. Gascon, Fundamentals and applications of photo-thermal catalysis, *Chem. Soc. Rev.* 50 (2021) 2173–2210, <https://doi.org/10.1039/DQCS00357C>.
- [60] C. Song, Z. Wang, Z. Yin, D. Xiao, D. Ma, Principles and applications of photothermal catalysis, *Chem. Catal.* 2 (2022) 52–83, <https://doi.org/10.1016/j.chechat.2021.10.005>.
- [61] Y. Qi, Z. Yang, Y. Jiang, H. Han, T. Wu, L. Wu, J. Liu, Z. Wang, F. Wang, Platinum–copper bimetallic nanoparticles supported on TiO₂ as catalysts for photo–thermal catalytic toluene combustion, *ACS Appl. Nano Mater.* 5 (2022) 1845–1854, <https://doi.org/10.1021/acsanm.1c03429>.